DSP-Based Current Control with Dead-Time Compensation for Full-Bridge-Fed Permanent-Magnet Electrodynamic Shaker

Hung-Chi Chen, Yu-Ching Lin and Jhen-Yu Liao
Department of Electrical Engineering,
National Chiao Tung University, HsinChu, Taiwan.
hcchen@cn.nctu.edu.tw

***Abstract*—Permanent-magnet electrodynamic shaker (PMEDS) can be seen as a single-phase reciprocating machine and its equivalent circuit model are an inductance, a resistance and an induced voltage in series. The induced voltage of PMEDS is near zero as the current frequency is far from the resonant frequency and its maximum operating frequency is several kHz near ten times larger than that of rotating AC machine. From the result of analysis, the dead time in gate signals has large effect on the high-frequency current tracking performance. In this paper, the PI-type controller and simple dead-time compensation loop are used to improve the current tracking performance during the range from 10Hz to 2kHz. The proposed current control is implemented in the digital DSP-based system and the full-bridge converter is connected directly to PMEDS without any LC filter. The effectiveness of the proposed current control is verified by the provided simulation and measured results.**

I. INTRODUCTION

Shaking systems which can replicate an actual situation are being widely used for the vibration-proof test [1]. An electrodynamic shaker (EDS) functions to deliver a force proportional to its armature current and thus, EDS has good features such as good linearity and a wide-frequency response. In the past years, many papers regarding EDS [2-10] had been published and their summaries are listed in Table I. EDS can be divided into permanent-magnet electrodynamic shaker (PMEDS) and separately-excited electrodynamic shaker (SEEDS).

Compared with rotating AC machine, EDS can be seen as a single-phase reciprocating machine. Thus, EDS' mechanical equation can be either a third-order equation [2] or a second-order equation [3-10] where the mechanical dynamic of a rotating machine is often modeled as a first-order equation. In addition, the maximum operating electrical frequency of EDS is 2kHz~5kHz which is ten times larger than the maximum operating electrical frequency in rotating machines.

In [2-3], PMEDS is supplied by conventional linear power supply. However, it is well known that the linear power supply has large size, large weight and low efficiency [11]. Compared with the linear power supply, the switch-mode power supply has the advantages of small size, small weight and high efficiency [11]. Therefore, switch-mode power supply has been used to drive EDS in [4-10], recently.

From Table I, Full-Bridge (FB) converters are the common topology used to power EDS. It is noted that a LC output filter is connected between FB converter and EDS in [4-9], but in [10], FB converter is directly connected to ES without any LC filter. LC filter is used to reduce the output voltage harmonic, but it is expensive, large volume and it must decrease the overall system efficiency.

Table I. Summary for electrodynamic shakers in papers

		[2-3]	[4-6]	[7-8]	[9]	[10]	here
PM EDS	V406 (5Hz~2kHz)	√	√			√	√
	St 5000/300 (20Hz~5kHz)				√		
SE EDS	V-300 (5Hz~4kHz)			√			
Linear power supply		√					
Switch-mode power supply			√	√	√	√	√
Topology	with LC filter		√	√	√		
	without LC filter					√	√
Control loop	current control		√			√	√
	voltage control			√	√		
	Analog		√	√		√	
	Digital				√		√
	frequency (kHz)		**50**	**80**	**12**	**25**	**50**

For the case of no LC filter in [10], the FB output current is exactly the armature current, and thus the EDS generating force can be controlled directly by tracking the armature current. But, for the case of connecting a LC filter, FB output current is the armature current plus the filter capacitor current and the FB output voltage is the sum of the armature voltage and the filter inductor voltage. Therefore, in order to control the reciprocation of EDS with a LC filter, either armature current control or armature voltage control can be found in [4-9]. Due to inserting a LC filter, more number of feedback signals and more complicated control loops can also be found in [4-9].

Since the maximum operating frequency of EDS is as high as several kHz, the switching frequency needs to be set as near twenty times larger than this maximum frequency. In [4-6]

and [7-8], the switching frequency is set as 50kHz and 80kHz, respectively. It is noted that in [9], the used EDS can be operated as high as 5kHz, but only experimental waveforms at 200Hz are provided due to its low switching frequency 12kHz.

In the digital implementation of control loop, the sampling frequency is often as high as switching frequency. Therefore, in the past, the control loops were implemented in analog circuit in [4-8, 10]. Recently, the control loop was implemented in digital circuit in [9], but only experimental waveforms at 200Hz are provided in [9].

The behavior of armature voltage and armature current can be modeled as series-connected circuit with an inductance, a resistance and an induced voltage which is similar to the behavior of AC machine. However, in AC machine, the induced voltage is proportional to the rotating speed and it is often regarded as the disturbance of current loop [12].

In the equivalent circuit of EDS, the induced voltage is not proportional to the current frequency. The closer the current frequency is to the resonant frequency (20~40Hz), the larger the amplitude of the induced voltage is. From the result of this paper, when the frequency of PMEDS V-406 is larger than 1kHz, the induced voltage is near zero and can be neglected in the control loop (i.e. no disturbance in control loop). Therefore, the PI-type controller is able to achieve closed current tracking performance at high-frequency range due to no disturbance in the loop.

However, note the interesting results in [10] that the closed armature current tracking performance at current frequency 100Hz was easily obtained by only PI-type controller, but the closed tracking performance are lost at current frequency 1kHz and 2kHz. It shows some key factor may degrade the current tracking performance at current frequency higher than 1kHz.

From the results of analysis in this paper, the key factor degrading the high-frequency tracking performance is found to be the design of dead-time in the gate signals. Dead-time is used to avoid the short-circuit condition in FB, but it has effect on the output voltage distortion [11]. In the low-frequency range, the effect of dead time on FB output voltage can be easily compensated by the PI-type controller. But in high-frequency range, PI-type controller is not able to compensate it due to the small number of PWM periods. In this paper, a simple dead-time compensation loop is included to PI-type controller to improve the current tracking performance especially at high-frequency range.

The paper is organized as follows. In first, the mechanism and governed equations of a PMEDS are studied. At the same time, the behavior of a FB with unipolar switching scheme and the resulting dead-time effect are also represented as several block diagrams. Then, the proposed current control is designed and implemented in a fully digital system. Finally, some simulation and experimental results have been given to demonstrate the performance of the proposed current control for PMEDS.

II. PERMANENT-MAGNET ELECTRODYNAMIC SHAKER

The cut-view plot of PMEDS is show in Fig. 1 where the permanent-magnet yields a constant and homogeneous flux density B at the air gap between the armature coil and iron core. The flowing direction of armature current i_a and the direction of air-gap flux density are perpendicular to one another. Thus, the generating force f_e of each conductor in the magnetic field is

$$f_e = NB\ell i_a = \Gamma i_a \tag{1}$$

where ℓ is the effective length of each conductor and N is the effective number of conductors in the magnetic field.

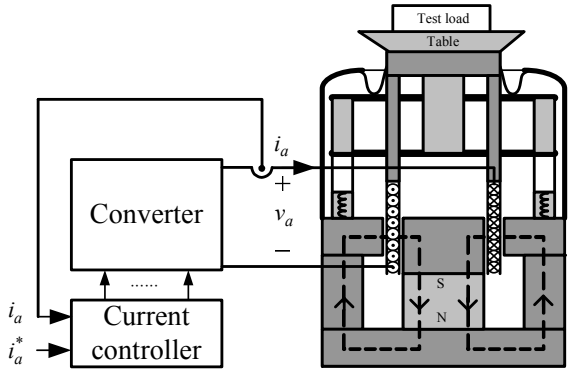

Fig. 1. Permanent-magnet electrodynamic shaker (PMEDS).

A. Mechanical Equation

Under the assumptions that the test load is free of resonances and rigidly attached to the table, the shake table moves very much like the one-degree-of-freedom (1DOF) system as shown in Fig. 2 and the mechanical governed equation can be easily expressed as

$$f_e = m\frac{d^2x}{dt^2} + c\frac{dx}{dt} + kx \tag{2}$$

where x is displacement of the movement of the shaker from standstill and m is the total mass of the movement plus the test load. k and c are the shaker suspension stiffness and damping coefficient, respectively.

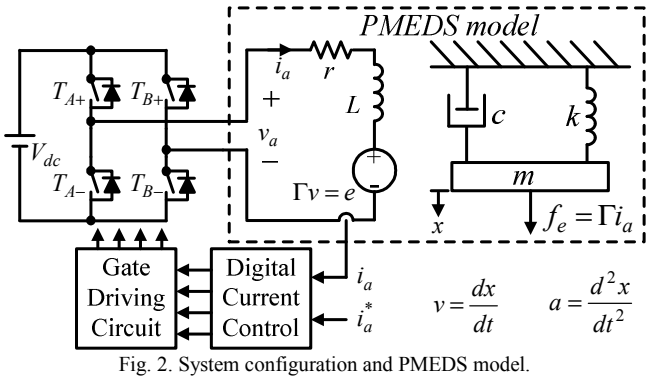

Fig. 2. System configuration and PMEDS model.

B. Electrical Equation

The conductor moving within the magnetic field would induce some voltage across each conductor and the lumped induced voltage e (i.e. back electromotive force, back-EMF) across the armature can be expressed.

$$e = \Gamma v = \Gamma \frac{dx}{dt} \tag{3}$$

Then, the KVL equation relating the armature voltage v_a to the armature current i_a can be obtained from Fig. 2.

$$v_a = r i_a + L \frac{di_a}{dt} + e \tag{4}$$

C. PMEDS Parameters

Since the used PMEDS V406 in this paper is the same as the one in [4-6], the estimation technique developed in [5] is applied as an alternative to find the parameters. The obtained nominal parameters are.

$$\begin{aligned} &\overline{m} = 0.245kg, \quad \overline{k} = 13143N/m, \\ &\overline{c} = 3.54N \cdot s/m, \quad \overline{\Gamma} = 12.3N/A \end{aligned} \tag{5}$$

where $\overline{m}$ is the estimated table weight. Thus, the resonant frequency of the shaker mechanical system without test load (no load condition) is near $\sqrt{\overline{k}/\overline{m}}/(2\pi) \approx 36.86Hz$. After fixing a load $0.311kg$ to the shaker table, the total weight of the moving one is increased to 0.532 kg, and the resonant frequency is reduced to near $25.02Hz$.

In [5], the estimated armature resistance $\overline{r}$ and inductance $\overline{L}$ at frequency $2kHz$ are

$$\overline{r} = 2.9\Omega, \quad \overline{L} = 0.1mH \tag{6}$$

The armature time constant of shaker system is near $\overline{L}/\overline{r} \approx 34.5\mu s$ which is much smaller than the winding time constants of common AC motors because that the shaker gap between the moving coil and the fixed iron is larger than the motor gap.

D. PMEDS Fed by Ideal Current Source

In order to understand no-load characteristics of PMEDS, the simulation results of a PMEDS fed by an ideal sinusoidal current sources (with unity amplitude 1A) are plotted in Fig. 3 where no load weight is fixed to the shaker table. When the current frequency is far smaller than the resonant frequency (near 36Hz) as shown in Fig. 3(a), both induced voltage e and the armature voltage v_a are smaller than 2V and the former is near $90°$ leading to the latter.

As the current frequency is closed to the resonant frequency (near 36Hz) in Fig. 3(b), the induced voltage e grows due to the resonance effect and the armature voltage v_a is almost equal to the induced voltage e (i.e. in phase). As shown in Fig. 3(c), the current frequency is larger than the resonant frequency (near 36Hz), both induced voltage e and the armature voltage v_a decreases and the former is near $90°$ lagging to the latter. From Fig. 3(d), Fig. 3(e) and Fig. 3(f), the larger the current frequency becomes than the resonant frequency, the smaller the induced voltage e is.

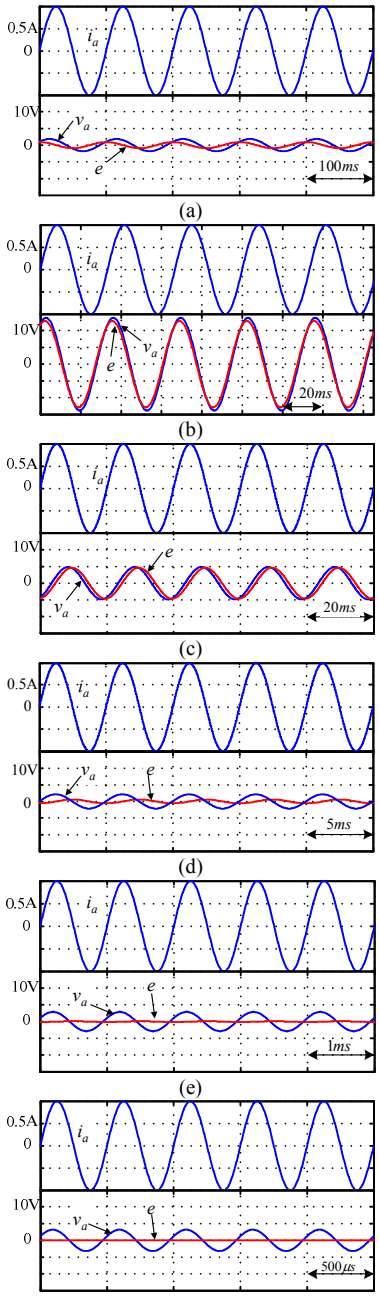

Fig. 3. Simulation no-load results of PMEDS fed by ideal current source: (a) 10Hz/1A; (b) 30Hz/1A; (c) 50Hz/1A; (d) 200Hz/1A; (e) 1kHz/1A; (f) 2kHz/1A.

In addition, the simulation results of a PMEDS with load 0.311 kg are plotted in Fig. 4. The significant difference in induced voltages of Fig. 3(b) and Fig. 4(c) can be found. At 30Hz, the peak of the induced voltage e is near 4V in Fig. 4(c), but the induced voltage e in Fig. 3(b) is near 14V.

From (5), it is cleared that the maximum peak of the induced back-EMF e will be near $(\Gamma^2/c) \approx 42$ times the peak current amplitude at the resonant frequency. Therefore, for sinusoidal current waveform with unit amplitude (1A), the peak value of induced back-EMF is near 42V, and thus, the

dc link voltage of the FB converter must be greater than 42V and is chosen $V_{dc} = 80V$ in this paper.

Fig. 3 and Fig. 4 show that the added load on shaker table has the effect on the induced voltage e when the current frequency is near the resonant frequency. Fig. 3 and Fig. 4 also show that the induced voltage is near zero and can be neglected at the frequency far from the resonant frequency (i.e. the high-frequency range).

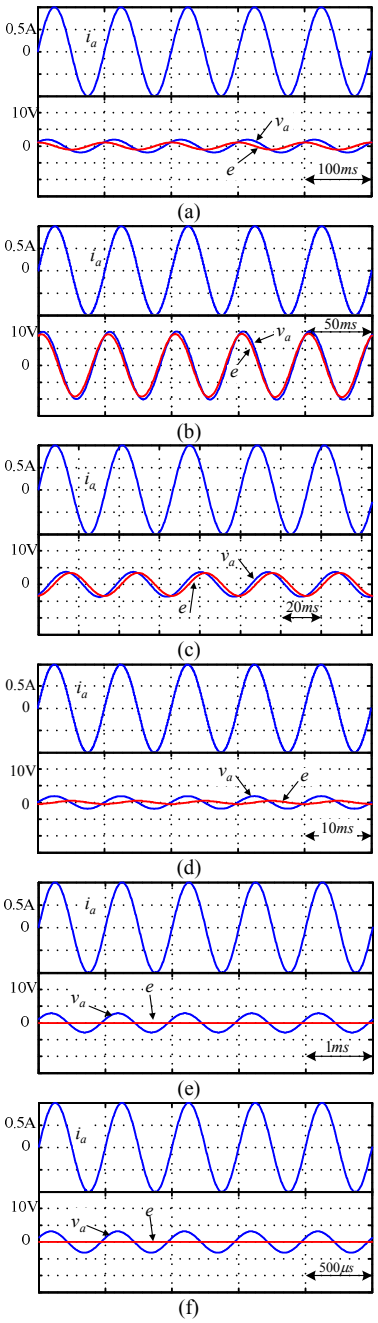

Fig. 4. Simulation results of PMEDS (0.311kg) fed by an ideal current source: (a) 10Hz/1A; (b) 20Hz/1A; (c) 30Hz/1A; (d) 100Hz/1A; (e) 1kHz/1A; (f) 2kHz/1A.

III. Modeling of Full-Bridge-Fed PMEDS

A. Unipolar Switching Scheme

As shown in Fig. 2, the FB topology is used to generate output voltage v_a. For PMEDS application, the frequency of armature current may be up to 2kHz. Due to limitation of switching frequency of practical semiconductor device, the unipolar switching scheme with characteristic of double PWM frequency is used in this paper. In order to avoid the short-circuit condition, adequate dead-time between the gate signals is necessary and the effect of dead-time on the voltage distortion should be studied.

B. Effect of Dead Time

In order to understand the effect of dead time on the output voltage, the gate signals and the resulting output voltage without dead time and with dead time t_Δ are plotted in Fig. 5(a) and Fig. 5(b), respectively.

When the armature current $i_a > 0$ is positive, the resulting average voltage $\bar{v}_a$ in Fig. 5(b) is smaller than the ideal average voltage $\bar{v}_a$ in Fig. 5(a) with $V_{dc} f_{PWM} t_\Delta$ where f_{PWM} is the PWM frequency. Contrarily, the resulting average voltage $\bar{v}_a$ in Fig. 5(b) is larger than the ideal average voltage $\bar{v}_a$ in Fig. 5(a) with the amplitude $V_{dc} f_{PWM} t_\Delta$ due to the negative armature current $i_a < 0$. Therefore, the dead-time effect on output voltage can be represented as

$$\Delta\bar{v}_a = -2sign(i_a) V_{dc} f_{PWM} t_\Delta \tag{7}$$

where $sign(x)$ is a sign function.

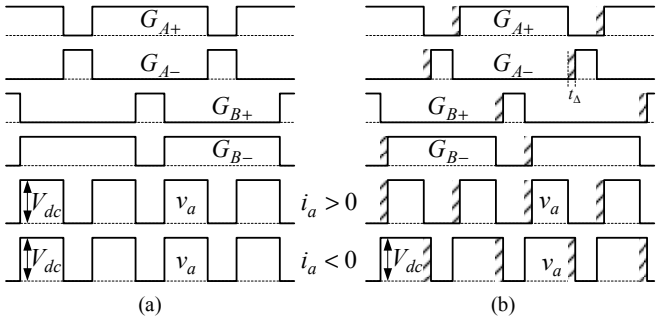

Fig. 5. Gate signals and the resulting armature voltage v_a: (a) without dead time t_Δ; (b) with dead time t_Δ.

With the unity carrier signal varying between +1 and -1, the average output voltage $\bar{v}_a$ can be represented as

$$\bar{v}_a = v_{cont} V_{dc} + \Delta\bar{v}_a \tag{8}$$

where v_{cont} is a signal compared with the carrier signal to generate the gate signals. From (1-4) and (7-8), the equivalent model for the full-bridge-fed PMEDS can be plotted in Fig. 6.

Generally speaking, the dead time t_Δ is selected according to the turning-on time and turning-off time on the datasheet of the used power switch. However, the maximum operating frequency of PMEDS is high to $2kHz$ and thus, the used PWM frequency f_{PWM} should be high enough to yield the closed current tracking performance. It means that the dead-time effect of PMEDS application is much larger than that of

other applications, such as motor driving. Thus, the dead-time compensation is included in the following digital current control to alleviate the dead-time effect.

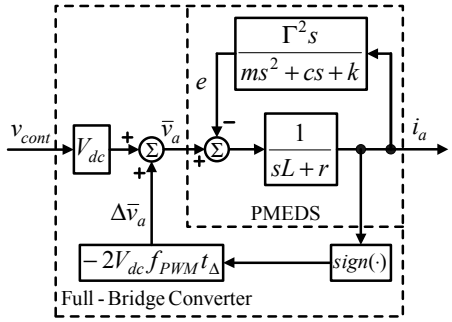

Fig. 6. Equivalent model for full-bridge-fed PMEDS.

Because of the used unipolar PWM scheme, the equivalent carrier frequency in the output voltage is twice the actual carrier frequency. By considering the maximum operating frequency 2kHz of the shaking test and the practical limitations of semiconductor switch, the PWM frequency is chosen as $f_{PWM} = 50kHz$ and the dead time is set as $t_\Delta = 0.5\mu s$.

C. Dead-Time Compesation

The derived transfer function of PMEDS from (1)-(4), the modeling of full-bridge converter from (7)-(8) and the proposed current control are plotted together in Fig. 7.

From Fig. 7, the equivalent dead-time voltage $\Delta\bar{v}_a$ can be concealed by adding the compensation component v_c . Then, the average armature voltage $\bar{v}_a$ can be expressed as

$$\bar{v}_a = v_{PI} V_{dc} \tag{9}$$

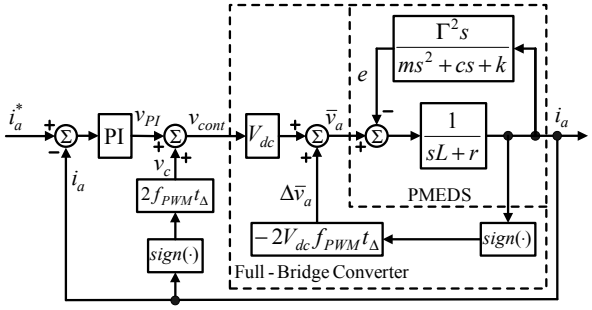

Fig. 7. Proposed current control for PMEDS.

IV. Simulation Results

A. Fed by only PI Feedback Current Control

In order to understand current tracking performance of PMEDS with only feedback loop (i.e. without dead-time compensation loop), the no-load simulation results with current command 10Hz/1A, 30Hz/1A, 50Hz/1A, 200Hz/1A, 1kHz/1A and 2kHz/1A are plotted in Fig. 8(a), Fig. 8(b), Fig. 8(c), Fig. 8(d), Fig. 8(e), and Fig. 8(f), respectively.

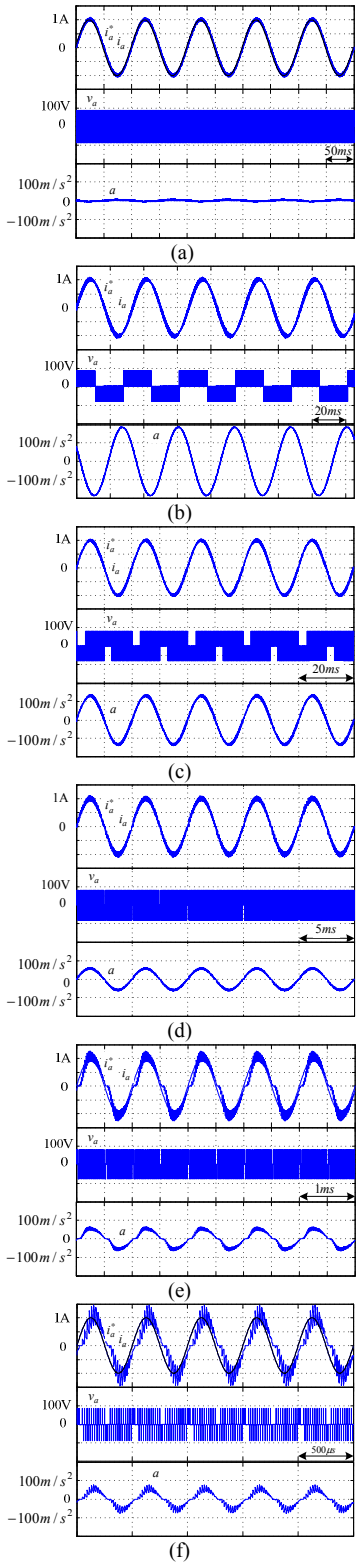

Fig. 8. No-load simulation results with only PI feedback loop: (a) 10Hz/1A; (b) 30Hz/1A; (c) 50Hz/1A; (d) 200Hz/1A; (e) 1kHz/1A; (f) 2kHz/1A.

It is cleared that the yielded PMEDS current i_a is closed the current command i_a^* in the low-frequency range even

when the command frequency is closed to the resonant frequency (near 36.86Hz) as shown in Fig. 8(c) and Fig. 8(d).

It is easy to observe the current ripple from Fig. 8(f) because in the high PMEDS frequency range, the corresponding PWM number of each cycle is low. It also means that it is not easy to remove the PWM dead-time effect within several PWM cycles. Thus, even though the PMEDS induced voltage is near zero as shown in Fig. 3(e) and Fig. 3(f), the PI feedback loop is not able to yield closed current tracking performance as shown in Fig. 8(e) and Fig. 8(f).

B. Fed by PI Loop and Dead-Time Compesation Loop

In order to obtain closed current tracking performance in the overall frequency range of shaking test, dead-time compensation loop is added. The no-load simulation results for current commands 1kHz/1A and 2kHz/1A are plotted in Fig. 9(a) and Fig. 9(b), respectively. Compared with Fig. 8(e) and Fig. 8(f), the closed current tracking performance is obtained after including the dead-time compensation loop.

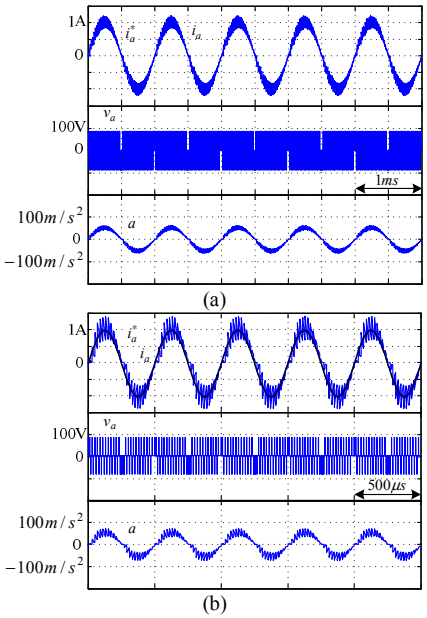

Fig. 9. Simulation results with PI feedback loop and dead-time compensation loop (a)1kHz/1A (no load); (b)2kHz/1A (no load),

V. EXPERIMENTAL RESULTS

The proposed current control has been digitally implemented in a DSP-based system using TMS320F2812 and all the experimental parameters had been listed in (5) and (6). As plotted in Fig. 10, both the sampling frequency of control loop and A/D conversion are 50kHz to keep with the PWM frequency. A accelerometer is mounted on the PMEDS table to monitor the acceleration signal a .

A. Steady-State Tracking Performance

The no-load experimental results with only PI-type feedback loop are plotted in Fig. 11. Fig. 11(a), Fig. 11(b), and Fig. 11(c) show closed current tracking performance, but the system loses the closed tracking performance at high-frequency range as shown in Fig. 11(d) and Fig. 11(e). The maximum acceleration rate measured by accelerometer is about 200 m/s^2 ($\approx 20g$) as shown in Fig. 11(a) when the frequency 30Hz is closed to the resonant frequency 36.86Hz.

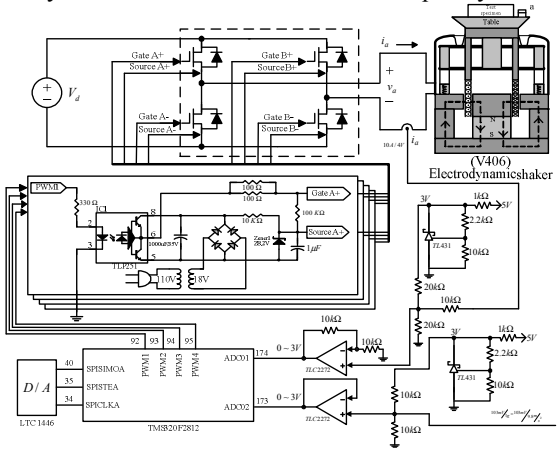

Fig. 10. The DSP-based experimental system.

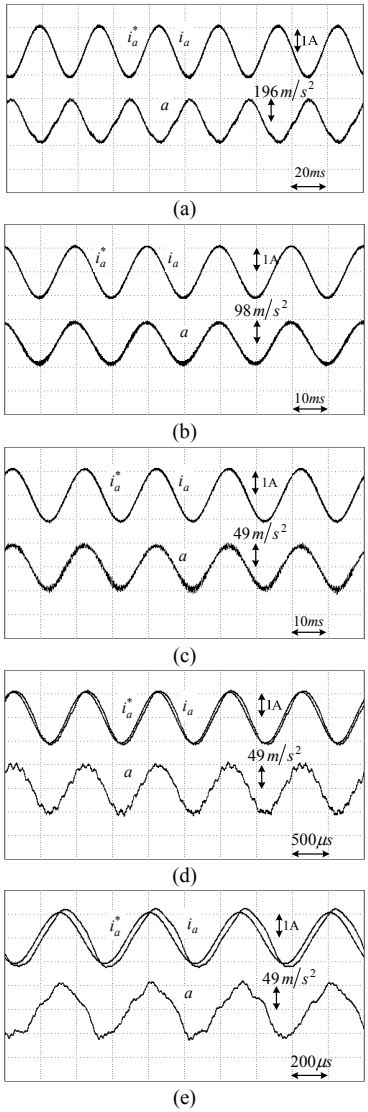

Fig. 11. No-load experimental results with only feedback loop: (a) 30Hz/1A; (b) 50Hz/1A; (c) 250Hz/1A; (d) 1kHz/1A; (e) 2kHz/1A.

The experimental results with load 0.311kg are plotted in Fig. 13 and similar results can be found. With only PI-type loop, the closed tracking performance can also be achieved at low-frequency range at Fig. 12(a), Fig. 12(b), and Fig. 12(c). But the closed tracking performance is also lost at high-frequency range as shown in Fig. 12(d) and Fig. 12(e). The maximum acceleration rate measured by accelerometer is about $98\,m/s^2$ ($\approx 10g$) as shown in Fig. 12(a) and Fig. 12(b) where the current frequency 20Hz and 30Hz are closed to the resonant frequency 25.02Hz.

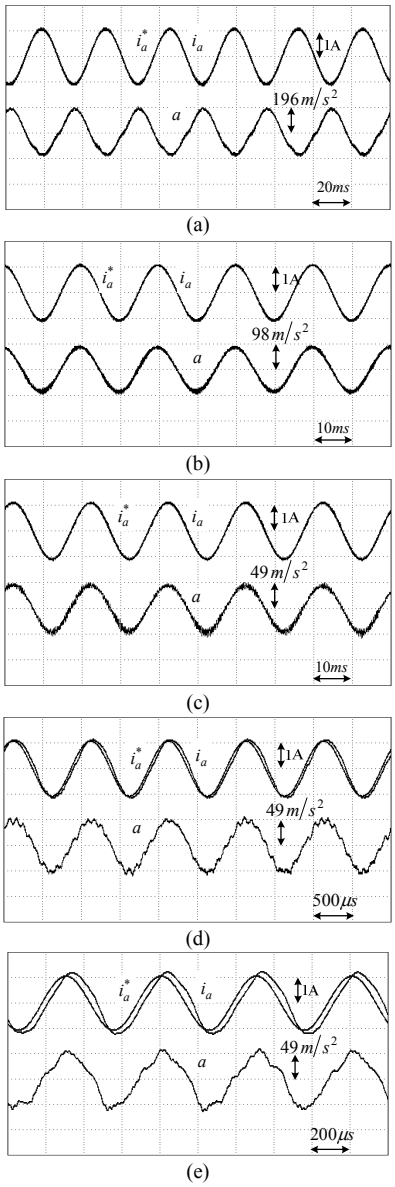

Fig. 12. Experimental results with only feedback loop (load 0.311kg), (a) 20Hz/1A; (b) 30Hz/1A; (c) 100Hz/1A; (d) 1kHz/1A; (e) 2kHz/1A.

Then, the no load experimental results with only feedback loop and a dead-time compensation loop at current command 1kHz/1A and 2kHz/1A are plotted in Fig. 13(a) and Fig. 13(b), respectively. The other waveforms in Fig. 13(c) and Fig. 13(d) are the load results (0.311kg) of adding dead-time compensation loop to PI current control loop. Obviously, the closed current tracking performances at high-frequency range are achieved by including the dead-time loop.

It is noted that obvious harmonics in acceleration a can be found in Fig. 13 even though the closed sinusoidal PMEDS current is yielded. Since one-resonant-frequency model is used in this paper, the simulated acceleration waveforms in Fig. 9 are near sinusoidal waveforms, but the measured acceleration waveforms in Fig. 13 carried some harmonics.

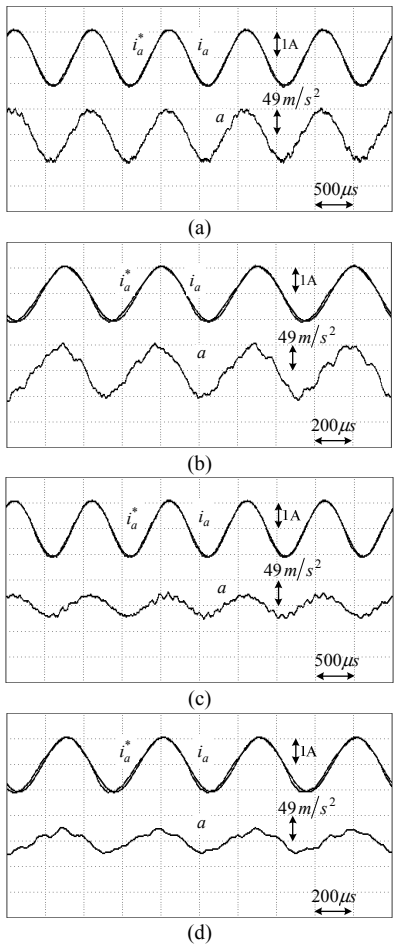

Fig. 13. Experimental results with PI feedback loop and dead-time compensation loop, (a)1kHz/1A (no load); (b)2kHz/1A (no load), (c)1kHz/1A (load 0.311kg); (d)2kHz/1A (load 0.311kg).

B. Transient Tracking Performance

In order to evaluate the performance of sweeping current command frequency, the experimental results without load and with load 0.311kg by linearly increasing the current command frequency are plotted in Fig. 14. The yielded armature current i_a is closed to the current command i_a^* and the measured no-load maximum acceleration rate is high to $490\,m/s^2$ ($\approx 50g$). However, the provided waveforms show that the simple PI loop and the dead-time compensation loop are able to provide closed current tracking performance during the operation frequency range of PMEDS.

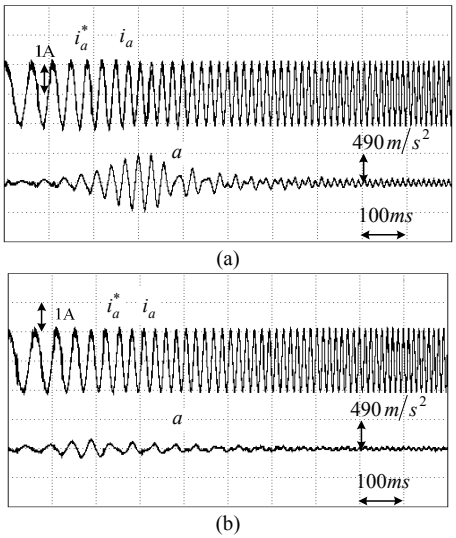

Fig. 14. Measured waveforms with sweeping command frequency (a) with no load; (b) with load $0.311kg$.

V. CONCLUSIONS

Modeling of FB-fed PMEDS has been studied and DSP-based current control has been designed and implemented in this paper. The results show that the dead-time has great effect on the high-frequency current tracking performance. A simple dead-time compensation loop is added to improve the current tracking performance especially in high-frequency range. From the simulation and experimental results, the closed current tracking performance is obtained by the proposed current control.

REFERENCES

[1] U. Koch, D. Wiedemann and H. Ulbrich, "Model-Based MIMO State-Space Control of a Car Vibration Test Rig with Four Electromagnetic Actuators for the tracking of Road Measurement," to be appeared in *IEEE Trans. on Industrial Electronics*, 2011.

[2] L. D. Flora and H. A. Grudling, "Time Domain Sinusoidal Acceleration Controller for an Electrodynamic Shaker," *IET Control Theory Appl.*, vol. 2, no. 12, pp. 1044–1053, Dec. 2008.

[3] Y. Uchiyama, M. Mukai and M. Fujita "Robust Acceleration Control of Electrodynamic Shaker Using μ-Synthesis," *in Proc. IEEE Conference on Decision and Control* (*CDC*), pp. 6170-6175, 2005.

[4] T. H. Chen and C. M. Liaw, "Vibration Acceleration Control of an Inverter-Fed Electrodynamic Shaker," *IEEE/ASME Trans. on Mechatronics*, vol. 4, no. 1, pp. 60-70, March 1999.

[5] B. J. Kang and C. M. Liaw, "Robust Hysteresis current-controlled PWM Scheme with Fixed Switching Frequency," *IEE Proc.-Electr. Power Appl.,* vol. 148, no. 6, pp. 503-512, Nov. 2001.

[6] C. M. Liaw, W. C. Yu and T. H. Chen, "Random Vibration Test Control of Inverter-Fed Electrodynamic Shaker," *IEEE Trans. on Industrial Electronics*, vol. 49, no. 3, pp. 587-594, June 2002.

[7] J. Han, T. Tang, and X. Wang, "A High-Performance Switching Mode Power Amplifier for Electrodynamic Shaker," *in Proc. IEEE International Conference on Industrial Technology* (*ICIT*), pp. 491-495, 2005.

[8] J. Han, T. Tang, and X. Wang, "Sinusoidal Vibration Test Control of a Switching Mode Power Amplifier-Fed Electrodynamic Shaker," *in Proc. IEEE International Conference on Industrial Electronics and Applications* (*ICIEA*), pp. 1-5, 2006.

[9] L. D. Flora and H. A. Grudling, "Acceleration Control of an Inverter-fed Electrodynamic Shaker," in *Proc. IEEE Power Electronics Specialists Conference* (*PESC*), pp. 2799–2805, Jeju, Korea, June 2006.

[10] T. H. Chen, K. C. Huang and C. M. Liaw, "High-Frequency Switching-Mode Power Amplifier for Shaker Armature Excitation," *IEE Proc.-Electr. Power Appl.,* vol. 144, no. 6, pp. 415-422, Nov. 1997.

[11] N. Mohan, T. M. Undeland, and W. P. Robbins, *Power Electronics: Converter, Applications and Design,* 2nd ed. New York: Wiley, 1995.

[12] M. C. Chou and C. M. Liaw, "Development of Robust Current 2-DOF Controllers for a Permanent Magnet Synchronous Motor Drive with Reaction Wheel Load", *IEEE Trans. on Power Electronics*, vol.24, no. 5, pp. 1304-1320, 2009.

[13] L .Chen and F. Z. Peng, "Dead-Time Elimination for Voltage Source Inverters," *IEEE Trans. on Power Electronics*, vol.23, no. 2, pp. 574-580, March 2008.